POLITECNICO DI TORINO
Repository ISTITUZIONALE

Distinguishing Suspicious Brugada from Benign RBBB: Binary and Multi-Class Evaluation with a Lightweight CNN on Leads V1 and V6

Original
Distinguishing Suspicious Brugada from Benign RBBB: Binary and Multi-Class Evaluation with a Lightweight CNN on Leads V1 and V6 / Casella, A., Randazzo, V., Giustetto, C., Gaita, F., Pasero, E.. - ELETTRONICO. - (2026), pp. 1-6. (IEEE International Instrumentation and Measurement Technology Conference I2MTC 2026 Nancy (Fra) 25-28 May 2026) [10.1109/i2mtc66907.2026.11694974].

Availability:
This version is available at: 11583/3016025 since: 2026-09-28T14:47:24Z

Publisher:
IEEE

Published
DOI:10.1109/i2mtc66907.2026.11694974

Terms of use:

This article is made available under terms and conditions as specified in the corresponding bibliographic description in the repository

Publisher copyright
IEEE postprint/Author's Accepted Manuscript

©2026 IEEE. Personal use of this material is permitted. Permission from IEEE must be obtained for all other uses, in any current or future media, including reprinting/republishing this material for advertising or promotional purposes, creating new collecting works, for resale or lists, or reuse of any copyrighted component of this work in other works.

(Article begins on next page)

18 November 2026

Distinguishing Suspicious Brugada from Benign RBBB: Binary and Multi-Class Evaluation with a Lightweight CNN on Leads V_1 and V_6

Alessandro Casella
DET
Politecnico di Torino
Turin, Italy
alessandro.casella@polito.it

Vincenzo Randazzo
DET
Politecnico di Torino
Turin, Italy
vincenzo.randazzo@polito.it

Carla Giustetto
Department of Medical Sciences
University of Turin
Città della Salute e della Scienza
Turin, Italy

Fiorenzo Gaita
Department of Medical Sciences
University of Turin
J Medical
Turin, Italy

Eros Pasero
DET
Politecnico di Torino
Turin, Italy
eros.pasero@polito.it

***Abstract*—Brugada Syndrome (BrS) is a genetic channelopathy creating an arrhythmogenic substrate, whereas Right Bundle Branch Block (RBBB) is a widespread and generally benign conduction delay. Despite their distinct etiology, they share a striking phenotypic mimicry on the electrocardiogram (ECG), specifically the rSR′ pattern in the right precordial leads (V_1–V_3), which poses a complex signal classification challenge. This study evaluates a beat-level convolutional neural network trained on raw morphology from leads V_1 and V_6 to classify four clinically relevant patterns: Diagnostic BrS, Suspicious BrS, RBBB, and Normal tracings. The 4-class model achieves high discriminative performance for polarized patterns (AUC 0.99 for Normal and 0.96 for Diagnostic Brugada computed on a 5-fold cross-validation), while the Suspicious class remains challenging in a multiclass setting due to overlap. A focused binary classifier successfully separates Suspicious BrS from RBBB (AUC 0.97), revealing a stable decision boundary between ambiguous and benign morphologies. Gradient-based attribution confirms V_1 as the dominant lead, consistent with clinical expectations, while comparative analysis against a standard V_1–V_3 baseline validates the critical contribution of the lateral lead V_6 in distinguishing benign conduction delays. Robustness experiments under gaussian noise show stable performance within clinically realistic conditions, supporting the potential use of this lightweight model for interpretable, scalable screening of Brugada-like patterns, even in low-quality or digitized ECG recordings.**

***Index Terms*—ECG classification, Brugada diagnosis, right bundle branch block, convolutional neural network.**

I. Introduction and Related Works

Automated classification of cardiac diseases via electrocardiographic analysis represents one of the most complex challenges in biomedical engineering. Specifically, Brugada Syndrome (BrS), a channelopathy associated with risk of sudden cardiac death, poses unique metrological difficulties due to the temporal variability and subtlety of its phenotypic markers [1], [2]. Recent studies highlights that the traditional approach (healthy vs sick) is insufficient to manage the clinical complexity of BrS, necessitating classifiers capable of distinguishing between the diagnostic type-1 pattern, Right Bundle Branch Block (RBBB), and suspicious phenocopies [3].

The morphological overlap between RBBB and BrS, particularly the rSR′ pattern in right precordial leads, is the primary source of error in conventional algorithms [4], [5]. Fig. 1 provides representative electrocardiogram (ECG) segments for each diagnostic class, highlighting the morphological variability and potential overlap among them. Correctly identifying these patterns is critical for risk stratification in patients without previous cardiac arrest, as outlined in combined clinical-electrophysiological approaches [6]–[8]. Recent contributions have proposed three-class artificial intelligence (AI) models to improve sensitivity [9], while vision transformers have emerged as a breakthrough, treating ECG signals as images to capture long-range spatial dependencies for both diagnosis and fatal event prediction [10], [11].

Furthermore, AI can predict drug-induced type-1 patterns from standard ECGs, effectively identifying high-risk patients currently categorized as uncertain [12]. Pre-processing stage,

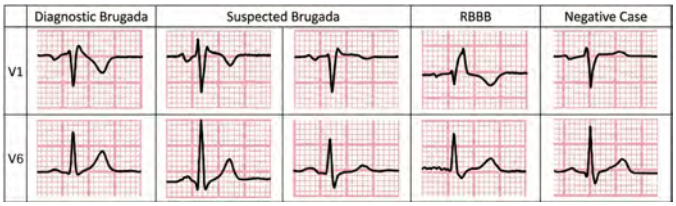


Fig. 1. Representative ECG beats for the four diagnostic classes (Diagnostic Brugada, Suspicious Brugada, RBBB, Normal) in leads V_1 and V_6. The visual overlap underscores the need for advanced differentiation.

involving accurate P-QRS-T segmentation and wavelet selection, is fundamental to extract consistent morphological features and ensure clinical reliability [13]–[16]. Parallel efforts in synthetic data generation and transfer learning are addressing the scarcity of labeled datasets for rare conditions [17], [18].

Our previous work introduced a binary classifier, later extended to three classes [9], but did not explicitly separate benign RBBB from risky Brugada patterns. This study proposes a four-class framework that disentangles Diagnostic Brugada, Suspicious Brugada, RBBB, and Normal morphologies, highlighting its value in distinguishing innocuous conduction delays from patterns suggestive of latent arrhythmic risk. The two proposed models (2-class and 4-class) specifically utilized leads V_1 and V_6 to exploit the diagnostic morphological dissociation between right precordial and lateral leads: while lead V_1 captures the specific R′-wave features necessary to identify Brugada-like patterns [19], the simultaneous analysis of lead V_6 allows for the detection of the deep slurred S-wave, the absence of which is a critical consensus criterion to distinguish BrS from true RBBB [20].

The remainder of this paper is organized as follows: Section II describes the data and network architecture; Section III presents the classification results and robustness analyses; and Section IV concludes with a clinical interpretation of findings and future directions.

II. Methods

A. Dataset and Study Population

The study dataset consists of 644 twelve-lead ECG recordings. A subset of 49 ECGs was originally available only on paper and was digitized from scans or photographs [21]. A set of 200 ECGs, only labeled as NORM (i.e., not associated with conduction blocks), was retrieved from the public PTB-XL database [22] to populate the Normal class. The other recordings were collected from several hospitals in the Piedmont region, Italy [23], [24], mainly using GE MAC 2000 and GE MAC 5 devices (GE HealthCare, Chicago, IL, USA). All ECGs were assigned to one of four diagnostic classes: Normal (no Brugada pattern and no RBBB), RBBB, Suspicious Brugada, and Diagnostic Brugada. This study was conducted according to the guidelines of the Declaration of Helsinki, and approved by the Institutional Review Board of Città della Salute e della Scienza Hospital, Turin, Italy (*Protocol code: 248/2017, date of approval: 22 February 2017*)

A patient-level split ensured that no subject appeared in more than one partition, using an 80–15–5% ratio for train, validation, and test sets. First, a scenario is considered with a hold-out test set containing medically representative ECGs and all others in the training/validation set. Since the test set is small to comply with the imposed proportions and therefore its performance would be considered non-generalizable, a stratified cross-validation was then performed, aggregating the results of the five different folds to calculate the global metrics.

Table I reports the ECG-wise distribution of the entire study cohort, with a representative split. The same stratified patient-level split was used for both the binary (RBBB vs. Suspicious Brugada) and the four-class configurations. No ECG appears in more than one partition. In the training, validation, and test sets, RBBB class represents approximately two-thirds of the samples and the Suspicious Brugada class approximately one-third, maintaining similar proportions and ensuring consistency between the different subdivisions of the dataset. In the four-class setting, the training set consists of 33.2% Normal, 38.4% RBBB, 20.4% Suspicious Brugada, and 8.0% Diagnostic Brugada samples, and these same class proportions are maintained in the validation and test sets.

TABLE I
ECG-wise class distribution in the split sets.

Split	Normal	RBBB	Suspicious	Diagnostic	Total
Train	171	198	105	41	**515**
Val	32	37	19	8	**96**
Test	11	13	7	2	**33**
Total	**214**	**248**	**131**	**51**	**644**

B. Beat Extraction and Preprocessing

All ECG signals were standardized to a uniform sampling rate of 1000 Hz. Native digital recordings were acquired at this original sampling frequency, while the digitized subset was resampled using piecewise cubic Hermite interpolation to preserve waveform monotonicity. Preprocessing involved two steps: first, baseline wander was removed by subtracting a low-frequency trend estimated via a 2nd-order Butterworth filter (0.5 Hz cutoff). Second, high-frequency noise was mitigated using a zero-phase low-pass filter with a cutoff frequency of 40 Hz. This cutoff was specifically selected to ensure spectral consistency across the heterogeneous dataset (aligning with the bandwidth of the legacy acquisitions), while fully preserving the macroscopic morphological features (e.g., ST-segment elevation, QRS widening) essential for Brugada and RBBB diagnosis. Beat extraction was based on the morphology of lead V_1, whose terminal S-wave provides a reliable landmark for both Brugada-like and conduction delay patterns. A wavelet-based enhancement followed by adaptive peak selection identified candidate S-points. Each detected beat was then segmented by extracting a fixed temporal window of 300 ms before and 550 ms after the S-peak, yielding a standardized 850-sample segment. To avoid redundancy, highly overlapping or nearly identical beats were automatically identified and removed using amplitude-based similarity criteria.

C. Neural Network Architecture

Fig. 2 illustrates the overall beat-level classification pipeline. The model operates directly on the raw morphology of beats extracted from leads V_1 and V_6, which provide the strongest discriminative information for separating Brugada-like patterns from RBBB (as discussed in Section I). No handcrafted features or inter-beat temporal context are used.

Each beat is processed by the *BeatFeatureExtractor*, a compact convolutional module composed of a sequence of 1-D convolutional layers with a kernel size of 3 and ReLU activation, each followed by batch normalization. These layers cap-

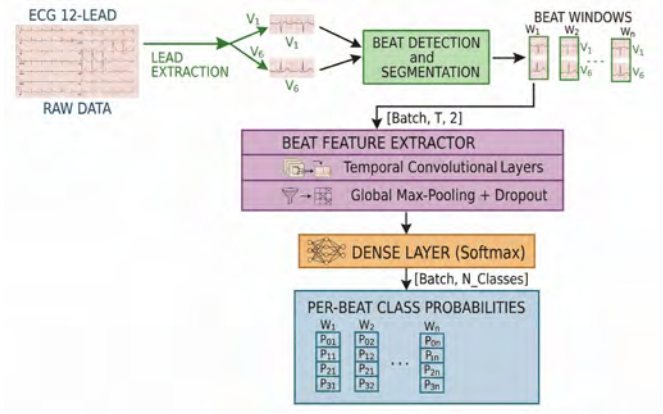


Fig. 2. Overview of the proposed beat-level classification pipeline from raw ECG signals to class probabilities.

ture local morphological patterns such as ST-segment elevation, rSR′-like configurations, and terminal conduction delays. To reduce dimensionality and prevent overfitting, each block concludes with a max-pooling layer ($size = 2$) and a dropout layer ($rate = 0.5$). The network employs a decreasing filter strategy with [128, 64, 32] filters respectively, concentrating capacity on low-level morphological features. A global max-pooling layer aggregates the temporal feature maps into a 32-dimensional latent vector before the final classification head. The resulting model contains approximately 100 k trainable parameters (see Table VII), ensuring lightweight deployment. The resulting feature vector is passed to a fully connected classification head with softmax activation, producing per-beat class probabilities. A final ECG-level prediction is obtained by averaging the softmax probabilities of all beats belonging to the same recording, as detailed in Section II-E.

D. Training Protocol

The preprocessing stage described in Section II-B produced a large beat-level dataset in which each beat inherits the class label of its parent ECG. Training was performed with a batch size of 64, using the Adam optimizer with a learning rate of 10^{-4}. The loss function was the sparse categorical cross-entropy. To mitigate class imbalance, balanced class weights were computed automatically from the training set and applied during optimization. Each model was trained for up to 100 epochs, with early stopping based on validation loss (patience = 10 epochs). No handcrafted data augmentation was applied. The only regularization mechanisms were dropout in the feature extractor, L_2 weight regularization, and additive Gaussian noise injected at the input of the *BeatFeatureExtractor* (defined in Section II-C). Training and validation pipelines employed TensorFlow pipelines with shuffling, caching, and prefetching to ensure reproducibility and high throughput.

Two configurations were trained: a binary classifier (RBBB vs. Suspicious Brugada) and a four-class model (Normal, RBBB, Suspicious Brugada, Diagnostic Brugada). Both models share the same architecture and training protocol, differing only in the number of output classes.

TABLE II
ECG-LEVEL PERFORMANCE OF THE 4-CLASS MODEL ON THE HOLD-OUT TEST SET.

Class	Precision	Recall	F1	Support
Normal	0.846	1.000	0.917	11
RBBB	1.000	0.846	0.917	13
Suspicious Brugada	0.583	0.500	0.539	7
Diagnostic Brugada	1.000	1.000	1.000	2

TABLE III
ECG-LEVEL PERFORMANCE OF THE BINARY MODEL ON THE HOLD-OUT TEST SET.

Class	Precision	Recall	F1	Support
RBBB	0.923	1.000	0.960	13
Suspicious Brugada	1.000	0.857	0.923	6

E. ECG-level Prediction

Each ECG signal was first segmented into individual beats, as explained in Section II-B. For every beat b_i, the beat-level classifier produced a softmax probability vector $\mathbf{p}(b_i) \in \mathbb{R}^K$, with K being the number of classes. To obtain a single prediction at ECG level, beat-level probabilities were averaged across the N_e beats of the recording, i.e., $\mathbf{p}(e) = \frac{1}{N_e} \sum_{i=1}^{N_e} \mathbf{p}(b_i)$. The final ECG label was then assigned as the class with highest mean probability: $\hat{y}(e) = \arg\max_k \; p_k(e)$.

All ECG-level performance metrics reported in this work (precision, recall, F1-score, and AUC) were computed using these aggregated predictions.

F. Evaluation Metrics

Model performance was assessed at both beat level and ECG level. Beat-level metrics quantify the discriminative ability of the backbone on individual segments, whereas ECG-level metrics are clinically meaningful, as final diagnoses rely on the interpretation of the entire tracing, especially relevant for intermittently manifesting conditions like Brugada. For each setting, accuracy, per-class precision, recall and F1-score, as well as macro- and weighted-F1 were reported. Receiver operating characteristic (ROC) curves and one-vs-rest AUC values are provided for the clinically relevant Brugada classes (see Sections III-A, III-B). To evaluate robustness, all metrics were computed on test data corrupted with additive Gaussian noise at multiple standard deviations (σ) (see Section III-D).

III. Experimental Results

A. ECG-Level Classification Performance

Table II reports the ECG-level classification performance of the four-class model on the hold-out test set. The model achieves strong discrimination for both the RBBB and Normal classes, with F1 scores of 0.917 for each. The very high performance on the limited Diagnostic samples available in the test set should be interpreted with caution due to the only two ECGs. As expected, the Suspicious Brugada class remains the most challenging, reflecting its intrinsic morphological variability and the overlap with RBBB-like and near-normal patterns. The model attains an F1 score of 0.539 for this class,

TABLE IV
CROSS-VALIDATION PERFORMANCE: BASELINE (LEADS V_1–V_3) VS. PROPOSED (LEADS V_1, V_6)

	Baseline Model (V_1, V_2, V_3)				Proposed Model (V_1, V_6)			
Class	**Avg. Supp.**	**Precision**	**Recall**	**F1-Score**	**Avg. Supp.**	**Precision**	**Recall**	**F1-Score**
Normal	113	0.91 ± 0.03	0.94 ± 0.06	0.92 ± 0.03	107	0.92 ± 0.08	$\mathbf{0.95 \pm 0.03}$	$\mathbf{0.94 \pm 0.05}$
RBBB	140	$\mathbf{0.99 \pm 0.02}$	0.91 ± 0.01	0.95 ± 0.01	141	0.96 ± 0.06	$\mathbf{0.95 \pm 0.05}$	$\mathbf{0.96 \pm 0.05}$
Suspicious BrS	55	0.62 ± 0.10	0.63 ± 0.09	0.59 ± 0.04	63	0.55 ± 0.22	0.64 ± 0.23	0.58 ± 0.22
Diagnostic BrS	14	0.65 ± 0.04	0.71 ± 0.14	0.68 ± 0.07	16	$\mathbf{0.85 \pm 0.14}$	$\mathbf{0.76 \pm 0.16}$	$\mathbf{0.80 \pm 0.14}$
Macro Avg	322	0.79 ± 0.09	0.80 ± 0.12	0.79 ± 0.06	327	$\mathbf{0.82 \pm 0.18}$	$\mathbf{0.82 \pm 0.17}$	$\mathbf{0.82 \pm 0.12}$
Accuracy	0.878 ± 0.03 (87.8%)				$\mathbf{0.900 \pm 0.05}$ (90.0%)			

consistent with the ambiguity inherent to its clinical definition. This behavior mirrors the structure observed in the t-SNE feature projection (see Section III-E).

Compared to the four-class configuration, the binary model displays significantly higher accuracy in separating RBBB from Suspicious Brugada. Table III reports the ECG-level performance of the binary model. The classifier achieves F1 scores of 0.960 for RBBB and 0.923 for Suspicious Brugada, with an AUC value of 0.968. The performance gap between the two models suggests that in the 4-class task, where Diagnostic and Suspicious Brugada patterns may overlap, the current backbone-only architecture lacks the capacity to fully disentangle these classes. This supports prior findings [9], where temporal attention via biLSTM proved more effective in capturing subtle diagnostic cues.

B. Impact of Lead Selection: Cross-Validation Comparison

A stratified 5-fold cross-validation was performed at beat-level to overcome the limitations of a single train-test split and evaluate the contribution of the lateral lead V_6.

Table IV contrasts the performance of the proposed 2-lead architecture (V_1, V_6) against a standard 3-precordial-lead baseline (V_1–V_3). For each class, the test set support (Avg. Supp.) is reported as the average value over the five folds. The proposed model achieved a higher overall accuracy ($90.0\% \pm 0.05$) compared to the baseline ($87.8\% \pm 0.03$). A substantial performance gain was observed in the Diagnostic Brugada class: the inclusion of lead V_6 increased the F1-score from 0.68 (Baseline) to 0.80 (Proposed), indicating a reduction in false negatives for high-risk patterns. The Suspicious Brugada class proved to be the most challenging for both configurations (F1-scores ≈ 0.58–0.59), reflecting the morphological overlap with RBBB and Diagnostic Brugada.

However, the ROC curves in Fig. 3 demonstrate that the proposed model retains high discriminative power even for this class, achieving an AUC of 0.93. The discrepancy between the high AUC and the moderate F1-score suggests that while the model correctly ranks Suspicious beats, the decision boundary remains sensitive to the specific threshold applied. The discrimination of Normal and RBBB beats remained robust across both models (F1 > 0.94), confirming that the lightweight V_1, V_6 setup preserves the recognition of benign conduction delays.

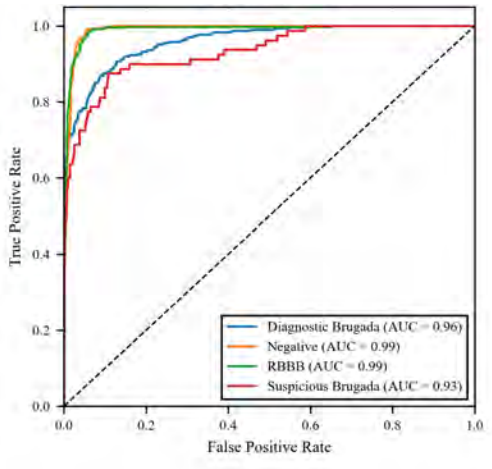


Fig. 3. ROC curves for the proposed model utilizing leads V_1 and V_6. The curves demonstrate the classification performance for each diagnostic class (Diagnostic Brugada, RBBB, Negative, Suspicious Brugada) computed by aggregating predictions from the 5-fold cross-validation. The AUC for each class is reported in the legend.

C. Confidence Analysis

Model reliability was evaluated by analyzing the distribution of beat-level predicted probabilities. For the Diagnostic Brugada class, true positives receive high confidence ($\mathbb{P} \approx 1$), while non-diagnostic traces cluster near zero. This polarized separation suggests that type-1 patterns have distinctive morphological features that the network detects with high certainty, consistent with the high F1-score (see Table IV). The Suspicious Brugada class shows a more heterogeneous probability spread, with many true beats assigned intermediate scores (e.g., 0.4–0.7), although RBBB mimics are largely suppressed near zero. This pattern reflects real biological ambiguity: suspicious morphologies form a continuum between normal and clearly pathological, so the model's spread-out confidence is expected.

D. Robustness to Gaussian Noise

Table V shows beat-level performance of the 4-class model under increasing Gaussian noise. The model remains highly robust for clinically realistic perturbations ($\sigma \leq 0.01$), maintaining macro-F1 above 0.84 and preserving diagnostic performance on both Suspicious and Diagnostic Brugada patterns.

TABLE V
ROBUSTNESS TO GAUSSIAN NOISE FOR THE 4-CLASS MODEL.

σ	$F1_{Norm}$	$F1_{RBBB}$	$F1_{Susp}$	$F1_{Diag}$	Macro-F1
0	0.960	0.957	0.730	0.718	0.841
0.01	0.959	0.930	0.696	0.778	0.841
0.05	0.000	0.564	0.000	0.000	0.141
0.10	0.000	0.565	0.027	0.000	0.148

However, performance degrades sharply for stronger noise ($\sigma \geq 0.05$), with F1 scores collapsing across all Brugada-related classes and also for the Normal class. In contrast, the RBBB class retains partial robustness, consistent with its more stereotypical and noise-resistant morphology.

E. Feature-Space Analysis

The beat-level t-SNE projection in Fig. 4 provides a qualitative view of the learned feature space. Negative (Normal) and RBBB beats are well separated along the vertical axis, forming distinct clusters in the lower and upper parts of the manifold, respectively. Diagnostic Brugada beats form a small but compact cluster in an intermediate region. In contrast, Suspicious Brugada beats populate multiple regions of the space: some points lie close to RBBB, others appear near Normal clusters, and a further group forms a compact island on the right-hand side. This wide dispersion confirms that Suspicious morphology spans a continuum between clearly normal and clearly pathological patterns, and explains the lower F1 score (see Table II) and the diverse misclassification patterns observed for this class.

F. Lead-Level Feature Relevance

Table VI compares the feature relevance assigned to leads V_1 and V_6 by the binary and 4-class models. Feature relevance scores were computed via gradient-based attribution, averaging the absolute input gradients with respect to the predicted class logits. Both models rely heavily on V_1, which carries most of the diagnostic information for Brugada and RBBB patterns. However, the binary model assigns relatively higher relevance to V_6, especially for Suspicious Brugada (14.4%), than the 4-class model (2.0%).

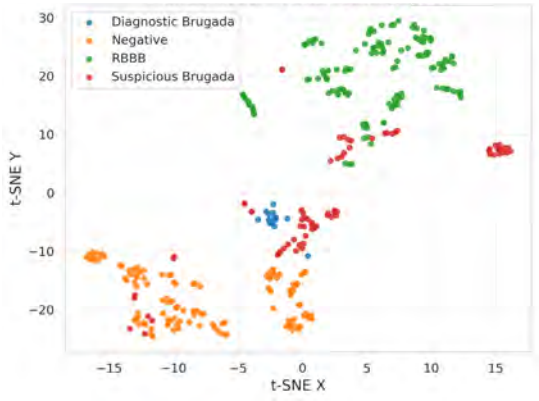


Fig. 4. t-SNE projection of beat-level features extracted by the 4-class model on the representative test set.

TABLE VI
GRADIENT-BASED FEATURE RELEVANCE (BEAT-LEVEL) FOR V_1 AND V_6.

Model	Class	Relevance V_1	Relevance V_6
Binary	RBBB	0.938	0.062
	Suspicious Brugada	0.856	0.144
4-class	Normal	0.960	0.040
	RBBB	0.925	0.075
	Suspicious Brugada	0.980	0.020
	Diagnostic Brugada	0.953	0.047

TABLE VII
COMPUTATIONAL COST OF THE BINARY AND 4-CLASS MODELS.

Model	Per-beat time [ms]	Beats/s	Batch time [s]	#Params
Binary	10.60	94.34	0.678	100,106
4-class	10.79	92.71	0.690	100,172

G. Computational Cost

Table VII reports the inference cost of the proposed models. Both architectures achieve real-time performance, processing more than 90 beats/s on a single GPU, with an average per-beat latency of approximately 10.6 ms. The 4-class model introduces only a negligible increase in computational load compared to the binary version, despite its higher output dimensionality. The parameter count remains close to 100 k in both cases, confirming that the network is lightweight and suitable for embedded or point-of-care implementations.

IV. DISCUSSION AND CONCLUSIONS

This study investigates the automatic recognition of Brugada-like ECG patterns using a beat-level classifier trained on raw morphology from leads V_1 and V_6. The model achieves high accuracy in both 4-class and binary tasks (see Tables II-III). The Suspicious Brugada class, however, remains challenging due to its structural ambiguity and clinical uncertainty. As shown in the ROC analysis (see Fig. 3), the model achieves a high AUC (0.93) for this class, but the lower F1-score (see Table IV) indicates that establishing a precise cut-off between Suspicious and RBBB classes is clinically complex. Most misclassifications involve this class, often interpreted by the model as a more polarized condition (e.g., RBBB or Diagnostic Brugada), reflecting real-world diagnosis where even expert consensus may vary.

Compared to our previous work [9], which used leads V_1–V_3, biLSTM layers, and an attention mechanism to capture temporal dependencies, the current model relies on vertical convolutions only, allowing a controlled evaluation of morphology-driven features without the influence of temporal aggregation. Furthermore, it yields an architecture with fewer parameters by an order of magnitude (see Table VII), simplifying real-time inference.

A key finding of this study is the impact of lead selection. Compared to clinical standard approaches for Brugada diagnosis which use contiguous precordial leads (V_1–V_3), the cross-validation results (see Table IV) demonstrate that pairing the right precordial lead V_1 with the lateral lead V_6 yields superior performance (accuracy 90.0% vs 87.8%, see Table

IV). Excluding V_2 and V_3 reduces redundancy among right precordial leads, while adding V_6 provides a complementary lateral view that helps distinguish the deep slurred S-wave of benign RBBB from Brugada patterns. This broader right-to-lateral perspective improves Diagnostic Brugada detection ($\Delta F1 = +0.12$), indicating greater effectiveness than a localized V_1–V_3 focus for this stratification task.

Lead-level relevance (see Section III-F) further clarifies these findings. In the binary task, the model leverages V_6 more prominently, indicating that late depolarization cues help distinguish the stereotypical terminal S-wave of benign RBBB from early Brugada-like morphologies. In the 4-class setting, however, the network concentrates its attention on V_1, which carries most Brugada-specific information. This stronger reliance on a single lead reduces sensitivity to subtler inter-class variations and contributes to the difficulty in separating Suspicious from Diagnostic Brugada. Robustness analysis confirmed stable performance under realistic noise levels (see Section III-D), including on 49 ECGs digitized from paper. Combined with the model's efficiency, this supports deployment both in real-time and low-resource environments.

In conclusion, reliable discrimination between Suspicious Brugada and RBBB is feasible and effectively optimized by using just two orthogonal leads (V_1, V_6). While the 4-class setting reveals Brugada's complexity, the binary task (Suspicious Brugada vs. RBBB) highlights a stable decision boundary between benign and potentially risky morphologies. Future work will combine spatial and temporal perspectives, experimenting with the complete V_1–V_2–V_3–V_6 lead configuration and dynamic labeling to better capture the Brugada spectrum and its intermittent nature.

REFERENCES

[1] M. El Sayed, A. Goyal, and A. L. Callahan, "Brugada syndrome," in *StatPearls [Internet]*, StatPearls Publishing, 2023.

[2] B. H. Gottschalk, J. Garcia-Niebla, D. D. Anselm, B. Glover, and A. Baranchuk, "Methods for improving the diagnosis of a brugada ecg pattern," *Annals of Noninvasive Electrocardiology*, vol. 21, no. 2, pp. 210–213, 2016.

[3] M. Carrington, A. Creta, W. J. Young, M. Carrington, J. Henriques, R. Teixeira, L. Gonçalves, P. D. Lambiase, and R. Providência, "Defining electrocardiographic criteria to differentiate non-type 1 brugada ecg variants from normal incomplete rbbb patterns in the young scd-sos cohort," *Journal of Cardiovascular Electrophysiology*, vol. 33, no. 9, pp. 2083–2091, 2022.

[4] A. R. Peréz-Riera, C. Ferreira Filho, L. C. de Abreu, C. Ferreira, F. G. Yanowitz, F. Femenia, P. Brugada, and A. Baranchuk, "Do patients with electrocardiographic brugada type 1 pattern have associated right bundle branch block? a comparative vectorcardiographic study," *Europace*, vol. 14, no. 6, pp. 889–897, 2012.

[5] P. A. Chiale, H. A. Garro, P. A. Fernández, and M. V. Elizari, "High-degree right bundle branch block obscuring the diagnosis of brugada electrocardiographic pattern," *Heart Rhythm*, vol. 9, no. 6, pp. 974–976, 2012.

[6] F. Gaita, N. Cerrato, C. Giustetto, A. Martino, L. Bergamasco, M. Millesimo, L. Barbonaglia, P. Carvalho, D. Caponi, A. Saglietto, *et al.*, "Asymptomatic patients with brugada ecg pattern: long-term prognosis from a large prospective study," *Circulation*, vol. 148, no. 20, pp. 1543–1555, 2023.

[7] C. Giustetto, S. Drago, P. G. Demarchi, P. Dalmasso, F. Bianchi, A. S. Masi, P. Carvalho, E. Occhetta, G. Rossetti, R. Riccardi, *et al.*, "Risk stratification of the patients with brugada type electrocardiogram: a community-based prospective study," *Europace*, vol. 11, no. 4, pp. 507–513, 2009.

[8] F. Gaita, N. Cerrato, A. Saglietto, D. Caponi, L. Calò, and C. Giustetto, "The brugada syndrome: risk stratification," *European Heart Journal Supplements*, vol. 25, no. Supplement_C, pp. C27–C31, 2023.

[9] V. Randazzo, A. Casella, S. Caligari, F. Gaita, C. Giustetto, and E. Pasero, "A three-class ai model for brugada syndrome detection to improve diagnostic accuracy in ecg analysis," in *2025 IEEE Medical Measurements & Applications (MeMeA)*, pp. 1–6, IEEE, 2025.

[10] V. Randazzo, S. Caligari, E. Pasero, C. Giustetto, A. Saglietto, W. Bertarello, A. Averbuch, M. Marcus-Kalish, V. Zheludev, and F. Gaita, "A vision transformer model for the prediction of fatal arrhythmic events in patients with brugada syndrome," *Sensors*, vol. 25, no. 3, p. 824, 2025.

[11] Z. Wu and C. Guo, "Deep learning and electrocardiography: systematic review of current techniques in cardiovascular disease diagnosis and management," *BioMedical Engineering OnLine*, vol. 24, no. 1, p. 23, 2025.

[12] P.-A. Călburean, L. Pannone, C. Monaco, D. D. Rocca, A. Sorgente, A. Almorad, G. Bala, F. Aglietti, R. Ramak, I. Overeinder, *et al.*, "Predicting and recognizing drug-induced type i brugada pattern using ecg-based deep learning," *Journal of the American Heart Association*, vol. 13, no. 10, p. e033148, 2024.

[13] S. Caligari, V. Randazzo, F. Gaita, C. Giustetto, M. Millesimo, and E. Pasero, "A neural network approach for the prediction of arrhythmic events in patients with brugada syndrome via ecg features analysis," in *2024 IEEE 22nd Mediterranean Electrotechnical Conference (MELECON)*, pp. 329–333, IEEE, 2024.

[14] L. D'Alvia, E. Palermo, and Z. Del Prete, "Accuracy evaluation of ecg waves detection and segmentation," in *2024 IEEE International Instrumentation and Measurement Technology Conference (I2MTC)*, pp. 1–6, IEEE, 2024.

[15] Q. Xiao and C. Wang, "Adaptive wavelet base selection for deep learning-based ecg diagnosis: A reinforcement learning approach," *PloS one*, vol. 20, no. 2, p. e0318070, 2025.

[16] R. Manzo, A. Apicella, P. Arpaia, F. Caputo, and N. Moccaldi, "Real-time detection of skin-electrode adhesion based on embedded neural networks for bioimpedance spectroscopy," *IEEE Access*, 2025.

[17] K. Saleh, R. Hadadi, Y. Liang, A. Sau, J. Howard, J. Artico, J. Ware, P. Kanagaratnam, F. Ng, W. Bai, *et al.*, "Application of machine learning techniques to optimise for limited datasets in an ai-ecg model for brugada classification," *Europace*, vol. 27, no. Suppl 1, pp. euaf085–827, 2025.

[18] Y. Lai, J. Chen, Q. Zhao, D. Zhang, Y. Wang, S. Geng, H. Li, and S. Hong, "Diffusets: 12-lead ecg generation conditioned on clinical text reports and patient-specific information," *Patterns*, 2025.

[19] G. Serra, A. Baranchuk, A. Bayes-De-Luna, J. Brugada, D. Goldwasser, L. Capulzini, D. Arazo, A. Boraita, M.-E. Heras, J. Garcia-Niebla, *et al.*, "New electrocardiographic criteria to differentiate the type-2 brugada pattern from electrocardiogram of healthy athletes with r′-wave in leads v1/v2," *Europace*, vol. 16, no. 11, pp. 1639–1645, 2014.

[20] A. B. de Luna, J. Brugada, A. Baranchuk, M. Borggrefe, G. Breithardt, D. Goldwasser, P. Lambiase, A. P. Riera, J. Garcia-Niebla, C. Pastore, *et al.*, "Current electrocardiographic criteria for diagnosis of brugada pattern: a consensus report," *Journal of electrocardiology*, vol. 45, no. 5, pp. 433–442, 2012.

[21] V. Randazzo, E. Puleo, A. Paviglianiti, A. Vallan, and E. Pasero, "Development and validation of an algorithm for the digitization of ecg paper images," *Sensors*, vol. 22, no. 19, p. 7138, 2022.

[22] P. Wagner, N. Strodthoff, R.-D. Bousseljot, D. Kreiseler, J. Lunze, W. Samek, and T. Schaeffter, "Ptb-xl, a large publicly available electrocardiography dataset," *Scientific Data*, vol. 7, no. 1, p. 154, 2020.

[23] F. Gaita, N. Cerrato, A. Saglietto, and et al., "Long-term risk of arrhythmic events in brugada syndrome: insights from the piedmont brugada registry," *European Heart Journal Supplements*, vol. 25, pp. C27–C31, 2023.

[24] C. Giustetto, N. Cerrato, and et al., "Long-term follow-up of patients with brugada syndrome in the piedmont brugada registry," *Heart Rhythm*, vol. 11, no. 1, pp. 142–149, 2014.